UDC 543 . 5 . 053

Technical Report

Progress of Three-dimensional Atom Probe Techniques for Analysis of Steel Materials —Development of Atom Probe Specimen Preparation Techniques for Site-specific Regions—

Jun TAKAHASHI* Kazuto KAWAKAMI
Yukiko KOBAYASHI Junichi YAMADA

Abstract

Three-dimensional atom probe (3DAP) is a very powerful tool which can investigate atomic positions of all alloying elements in steel with lattice-spacing spatial resolution. However, the very small analysis volume of 3DAP has limited its application field. To meet the needs for atomic-scale analyses of steel materials, advanced preparation techniques of a needle specimen tip including a site-specific region of interest in the steel were originally developed, based on the lift-out method with focused ion beam (FIB) fabrication. The preferable form of the needle specimen was provided by electrostatic field calculation using a finite element method. As examples of application, the atomic scale observations of low-density phase interfaces, of specific depth positions in white etching layer on rail surface, and of high-strength steel wire surface along the specific direction were shown. The developed techniques of needle tip fabrication enabled atomic-scale observations of almost all the site-specific regions of interest in steel, which widely expanded the application field of 3DAP.

1. Introduction

The three-dimensional atom probe (3DAP) is a device for obtaining a 3D image of the spatial position of 10,000,000 or more atoms of the constituent elements of a metallic material with a spatial resolution on a lattice spacing level. With the 3DAP, it is possible to accurately study the position of any presence and the local concentration of each of the elements added to a metallic material.[1-3] In the analysis of steel materials in particular, the 3DAP is a very powerful tool since it allows for quantitative measurement, with atomic-level spatial resolution, of various phenomena (solid solution, precipitation, distribution, segregation, etc.) of all the alloying elements that directly influence the formation and characteristics of the steel structure. Recently, the techniques involved in the 3DAP

* Chief Researcher, D.Eng., Materials Characterization Research Lab., Advanced Technology Research Laboratories
20-1, Shintomi, Futtsu, Chiba

are collectively called atom probe tomography (APT), which is being applied not only to metallic materials but also to semiconductors and insulators thanks to the development of a technology for irradiation with laser pulses in place of voltage pulses.[4, 5)]

In this analytical method, since element types are determined by measuring the time of flight of field-evaporated ions, it is possible to separately measure all the elements from hydrogen to the heavier elements (including isotopes) and determine them with a spatial resolution on a lattice spacing level. On the other hand, since this method observes atoms directly, the region that can be observed in a single measurement is extremely small—20 nm × 20 nm × 100 nm. Because of this, the scope of application of the method has been very limited. Even with the latest wide-view 3DAP, the area of the observable field is no larger than 100 nm × 100 nm. When applied in the analysis of a steel material, for example, it permits observation of a region only 1/100 or less of the standard grain size (up to 10 μm) of steel.

Besides, unlike semiconductor silicon, steel as a material is not uniform in its crystal structure or composition. Because of its polycrystalline structure, steel contains grain boundaries and has many lattice defects, including dislocations. In addition, steel is not made up of a single phase: it often has a complex structure containing different phases (bainite, martensite, cementite, retained austenite, etc.). Steel also contains precipitates, nonmetallic inclusions, and other substances that are different from iron. There is even a difference in structure, specifically composition, between the surface and the interior of a steel. The uneven distribution and density of alloying elements and defects influence the mechanical properties of steel materials. Therefore, in order to understand the relationships between steel characteristics and manufacturing conditions, it was necessary to consider the regions from which the steel characteristics manifest themselves and to conduct a pinpoint measurement of these regions.

In order to meet these needs, it was essential to develop a needle specimen preparation technique that permits positioning of the target region within the field of observation with the 3DAP, that is, approximately 100 nm from the needle tip. Formerly, needle specimens were prepared mainly using an electrolytic polishing technique called random sampling. Since the advent of focused ion beam (FIB) equipment, however, technology for preparing specimens from local regions using FIB has been developed. Using such FIB technology, a study group at Oxford University quickly succeeded in 3DAP measurement of grain boundaries and metallic multilayer.[6-9)] With the aim of making the technology more sophisticated and more practical, we developed a new technology for preparing needle specimens by means of pinpoint sampling of the target region in steel by utilizing the lift-out method.[10, 11)] The new technology has made it possible to apply the 3DAP in entirely new fields of observation and has led to several pioneering research efforts.

In this paper, we present examples of the application of our needle specimen preparation technology in the field of steel metallurgy.

2. Experimental Apparatus

FIB equipment (Hitachi FB-2000A) with a micro-sampling device (lift-out device) was mainly used to prepare the needle specimens, and gallium (Ga) ions were irradiated with an acceleration voltage of 30 kV for specimen preparation and observation of SIM (scanning ion microscope) images. To protect and bond the material, tungsten (W) vapor deposition by FIB irradiation was used. The needle specimens prepared were observed under a transmission electron microscope (TEM: Hitachi H-8000). For 3DAP measurement and field ion microscope (FIM) observation, energy compensation-type 3DAP equipment (Oxford NanoScience, Ltd.) featuring a delay-line position-sensitive transducer was used. The measuring temperature, measuring voltage, and pulse ratio were 60 K to 80 K, 10 kV to 15 kV, and 20%, respectively.

3. Development of Needle Specimen Preparation Technology

In the preparation of needle specimens for the 3DAP, FIB has been used not only to work materials that can hardly be worked by electrolytic polishing, but also to prepare needle specimens of ordinary grain boundaries, etc. As described in the "Steel Technology and Nanotechnology" article in the Nippon Steel Technical Report 2004, when observed under a scanning ion microscope (SIM), a grain boundary was recognized by the phenomenon of channeling contrast whereby a difference in contrast occurs between crystal grains with different orientations, and an ion beam scanned in the form of a ring was irradiated in parallel with a needle-shaped specimen to fabricate a needle whose tip had a radius of curvature of 50 nm or less (**Fig. 1** (a)). By repeating the above FIB fabrication and TEM observation alternately, it was possible to prepare a needle specimen that contains a grain boundary within 100 nm from the needle tip in the measuring region.[9, 10)]

However, using the method described above, it was difficult to obtain the desired needle specimen from any site-specific region. Therefore, the lift-out method that had been used to prepare TEM specimens was utilized in the fabrication of needle specimens.[12, 13)] Specifically, as described in the Nippon Steel Technical Report 2004,[10)] we cut out a block containing the target grain boundary by FIB while observing the microstructure under an SIM, took it out

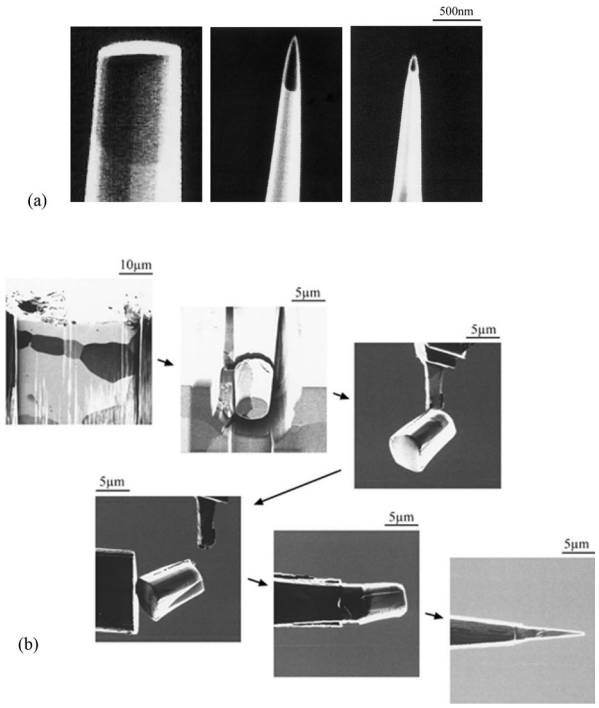

Fig. 1 Challenge to needle specimen fabrication of a site-specific region in steel[10)]
(a)FIB fabrication of needle specimen at grain boundary position, (b) Sampling of a site-specific region using lift-out method

using the lift-out method, and fixed it to the needle post (Fig. 1 (b)). Regarding this idea, we began pressing ahead with technological developments before a similar idea was proposed by another outside organization. Eventually, we established a process of preparing pinpoint needle specimens from site-specific regions ahead of the other research institutes.[11, 14-16)]

The process of preparing a needle specimen for pinpoint 3DAP observation is shown in **Fig. 2**. Here, the interface between different phases is taken as an example of a site-specific region. Ordinarily, steel consists of multiple phases (ferrite, martensite, cementite, etc.) and contains many lattice defects (dislocations, grain boundaries, etc.) and foreign matter (precipitates, nonmetallic inclusions, etc.). From the steel, a tiny columnar block containing the target interface between different phases is cut out by FIB in such a way that the interface comes to the front end of the block. The columnar block is carried to the needle post by a micromanipulator and fixed to the post by tungsten vapor deposition using FIB. The upper part of the block is then worked into a small square column by a Ga ion beam scanned in the form of a rectangle. After that, by irradiating a ring-shaped beam down from above the rectangular block, the block is worked in such a way that the grain boundary comes to within 100 nm of the needle tip.

In this needle specimen preparation process using the lift-out method, the needle specimen consists of two stages—the lower block and the upper block. This two-stage construction is advantageous from the standpoint of easy operation, strong bonding between the two stages, and short working time. However, the construction underwent a phenomenon whereby the field evaporation at the needle tip stopped halfway even when a voltage higher than the voltage assumed to be appropriate from the radius of curvature of the needle tip was applied. The reason for this was found to be that the field intensity at the needle surface is not determined simply by the radius of curvature of the needle tip but that it is significantly influenced by the construction of the entire needle specimen (including the lower block and the needle post).

Assuming the needle radius of the curvature and applied voltage to be r and V, respectively, electric field E at the surface of the needle specimen can generally be expressed by the following equation.

$$E = V / kr \quad (1)$$

here, k is a coefficient called the field factor, which is influenced by the needle shape and the needle specimen preparation equipment.[1)] It has been reported that the value of k for standard needle specimens prepared by the electrolytic polishing process is in the range of 2 to 8.[3, 16, 17)] If the value is particularly large, an electric field sufficient for field evaporation will not be formed on the needle surface even when a high voltage is applied.

Therefore, we studied the influence of the needle specimen shape on the field factor by an electrostatic field calculation using the finite element method.[11)] The inset in **Fig. 3** shows the shape of the needle specimen tip (block part) used in the above calculation. L is the distance from the needle tip to the upper surface of the lower block, and D is the diameter of the lower block. For the purpose of simplifying the calculation, the block was assumed to be cylindrical, not rectangular, and the radius of curvature at the needle tip and the diameter of the needle were set as 50 nm and 100 nm, respectively. Fig. 3 shows the calculated values of the field factor as a function of L/D. Here, the calculation results for several different block sizes are shown on the assumption that the size of the block cut out differs according to the size of the target region. Regardless of the block size, the field factor values obtained were dependent on L/D and approximately extrapolated by a straight line expressed by $k = 1.9/(L/D)^{0.9} + 2.5$.[11)]

The field factor value is strongly influenced by the boundary conditions used in the calculation. Under the same boundary conditions, however, it is possible to compare relative values. When the value of L/D is large ($L/D > 5$), the field factor values are in the range of 2 to 3. The reason that the values shown are somewhat smaller than those reported is probably that the shape of the specimen holder was left out of consideration.

When the value of L/D is small ($L/D < 5$), by contrast, the field factor value varies widely and the electric field at the needle speci-

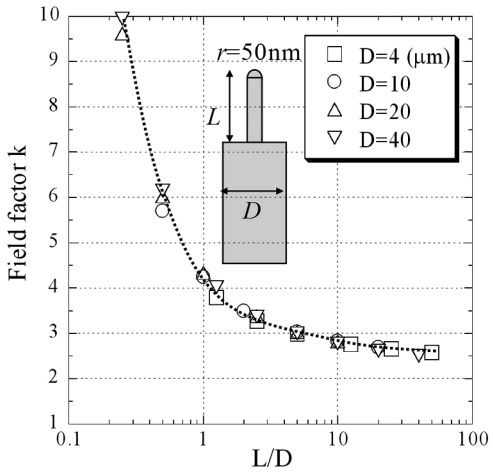

Fig. 3 Needle shape dependence of field factor calculated by the finite element method[11)]

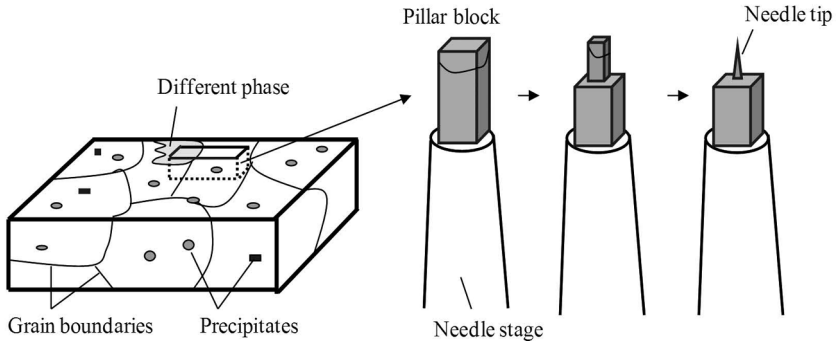

Fig. 2 Schematic drawing of needle specimen preparation process for the site-specific region analysis using lift-out method[11)]

men surface greatly depends on *L/D*. This indicates that with a decrease in needle length and with an increase in lower block diameter, the electric field at the needle specimen surface decreases markedly. It is understood that the reason for this is that the interference on the needle tip from the upper surface of the block at the same electric potential increases. On the basis of the above calculation results, we determined the desirable needle shape in the preparation of a specimen using the lift-out method. It is necessary that the milling region length, L, of the needle specimen should be at least twice the diameter, *D*, of the lower block.[11] In the present technological development, we prepared our needle specimens on the basis of electrostatic field calculations.

4. Application Examples of the Newly Developed Technology

4.1 Observation of the interface between different phases[11]

Ability to see the segregation and distribution conditions of alloying elements at the grain boundaries and at the interface between different phases provides extremely important information to better understand transformation and grain growth behaviors. These phenomena accompany changes in the local concentration of the alloying elements on a nanometer level. When it comes to measuring them, therefore, it is effective to use the 3DAP, since it has high spatial resolution and an excellent detection limit.

In this section, we describe an example of observing the interface between proeutectoid ferrite and bainite. The specimen was taken from a continuously cast slab whose composition was Fe-0.09C-1.6Mn-0.19Si (mass %). It was water-cooled from a temperature range of 800℃ to 900℃. The specimen had a bainite structure containing fine lath structures. In the temperature range of 800℃ to 900℃, proeutectoid ferrite grains occurred from the austenite grain boundaries, and the remaining austenite underwent a bainitic transformation in the cooling process. Therefore, the distribution of the alloying elements during the ferritic transformation was to be observed at the interface between the ferrite and the bainite. Since the target interface between the ferrite and the bainite was much lower in density than the interface between the bainite laths, etc., the technology for sampling a site-specific region described earlier was required.

Fig. 4 presents SIM images showing the process of preparing a needle specimen for observation of the interface between ferrite and bainite. In the SIM image of a nital-etched surface, the proeutectoid ferrite grains (α) show a plain contrast and can clearly be discriminated from the bainite grains (B) that show a complex contrast. As shown in Fig. 4, a square columnar block (10 μm × 10 μm × 80 μm) crossing the ferrite-bainite interface was cut out from the surface region using the FIB method. The block was fixed to the needle post, and the top of the block was made approximately 2 μm square by FIB. After that, the top of the block was made into a needle using a ring-shaped beam. Finally, the needle specimen was prepared in such a way that the target interface position was within 100 nm of the needle tip (see the photo inset in **Fig. 5** (a)).

Fig. 5 (a) shows 3D elemental maps of a ferrite-bainite interface region. The region measured is a box of 12 nm × 12 nm × 18 nm. In the figure, the solid line in the iron (Fe) map indicates the interface position. It can be seen that carbon (C) is noticeably concentrated in the bainite region. It can also be seen that manganese (Mn) is mark-

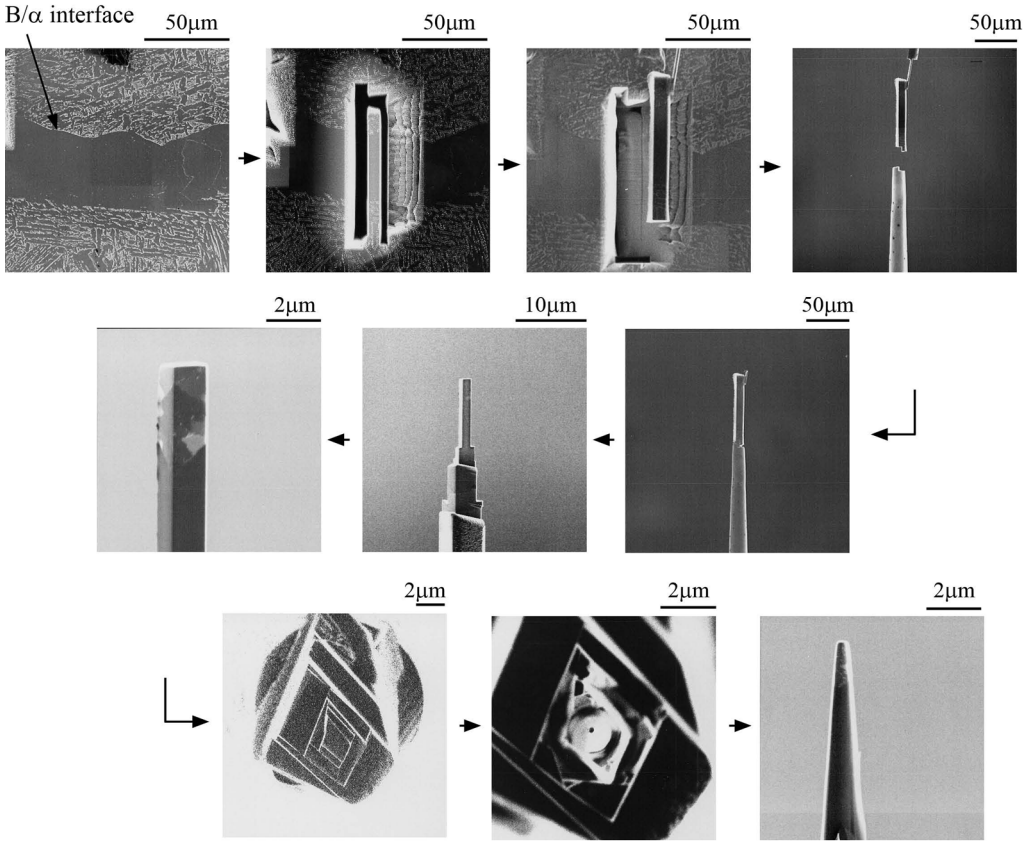

Fig. 4 Needle specimen fabrication process for atom probe analysis of the bainite-ferrite interface[11]

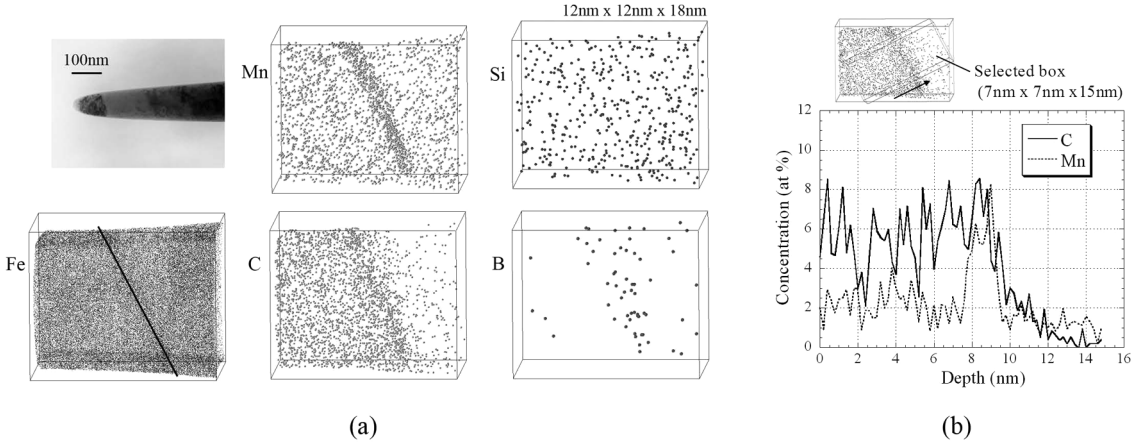

Fig. 5 3DAP analysis results of the bainite-ferrite interface
(a) 3D elemental maps (insert figure: TEM micrograph of the needle tip), (b) Carbon and manganese concentration profiles[11]

edly concentrated (segregated) in a 2-nm-wide region at the interface, and that silicon (Si) is evenly distributed throughout the interface. In addition, a small amount of boron (B) is observed in the neighborhood of the interface.

Fig. 5 (b) shows the concentration profiles of C and Mn in a direction perpendicular to the ferrite-bainite interface. The carbon concentration was about 6 at.% at the interface and gradually decreased in concentration in the direction of the bainite grains. The reason for this is thought to be that C was ejected into the austenite region during the formation of proeutectoid ferrite. The manganese concentration showed as much as 6 at.% at the interface position, but in the bainite region, it showed nearly the same concentration in the direction of depth. The ratio of Mn concentration between the ferrite region and the bainite region was about 0.58, which almost coincides with the ferrite-bainite distribution ratio at the retained temperature.[11]

The technology described above can be applied in quantitative observations of the distribution and segregation of elements at the interface between different phases, at specific grain boundaries, etc.

4.2 Observation of a steel wire surface in a direction perpendicular to lamellation[14, 18, 19]

Concerning high-carbon steel wire manufactured by subjecting high-carbon pearlitic steel to drawing and reinforcement, it has been reported that a large strain applied to the steel in the drawing process can break down the cementite in the steel and thereby adversely influence the characteristics of the product.[20] When it comes to discussing the breakdown of 1- to 2-nm-wide cementite lamellae and the carbon concentration in ferrite lamellae, it is effective to use the 3DAP. Incidentally, all the reports on high-carbon steel wire published in the past focus on measurements made in the direction of the steel wire (i.e., the direction of drawing).[21, 22] This is due to the fact that the needle specimens were directly prepared from thin steel wires by using the electrolytic polishing process. In a measurement using such a needle specimen, the spatial resolution of atoms in the direction perpendicular to the measuring direction was subject to deterioration caused by the local magnification effect.[1, 3] Besides, in the preparation of a needle specimen using the electrolytic polishing process, the measuring region was almost limited to the central part of the steel wire because the tip of the needle was positioned near the center of the steel wire. In particular, it is known that the carbon distribution in the surface region of the steel wire influences the characteristics of the wire.

Therefore, there has been strong demand for microscopic observation of the surface regions of steel wires. Under these conditions,

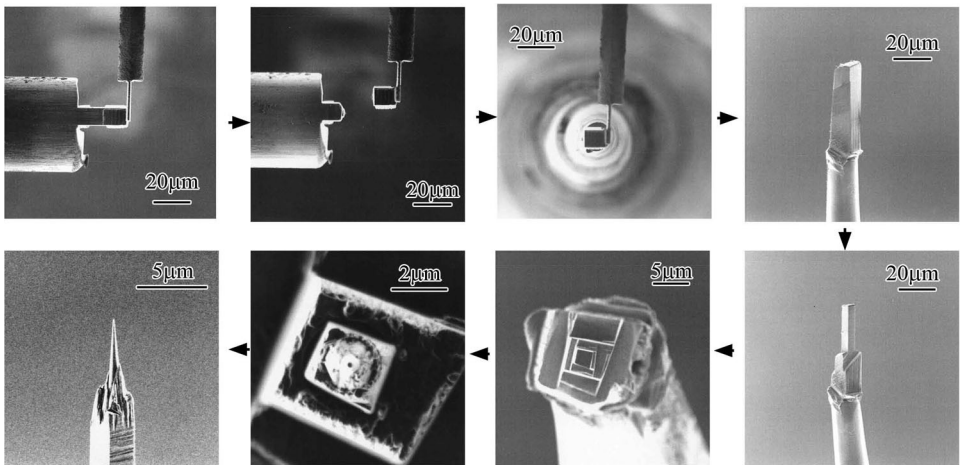

Fig. 6 Needle specimen fabrication process for atom probe analysis of high-strength wire surface along the direction perpendicular to the lamellae[19]

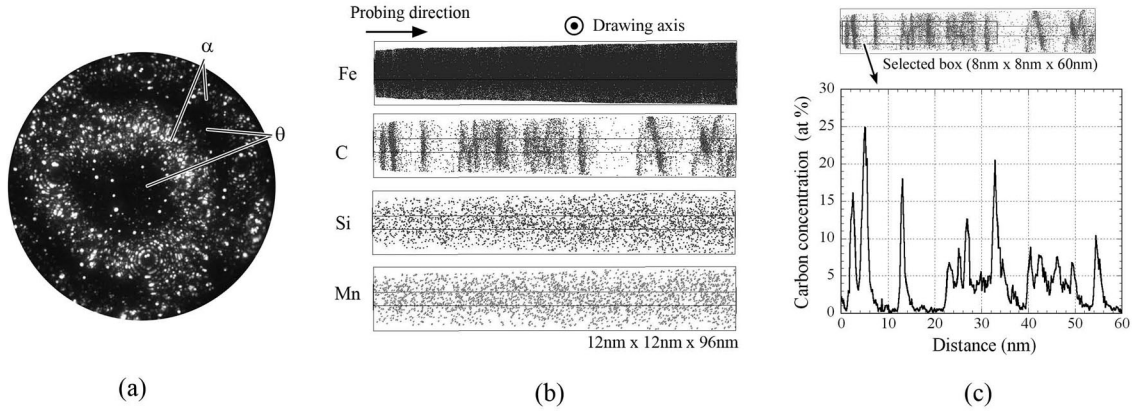

Fig. 7 3DAP analysis result of high-strength wire surface
(a) FIM image before probing, (b) 3D elemental maps, (c) Carbon concentration profile[19)]

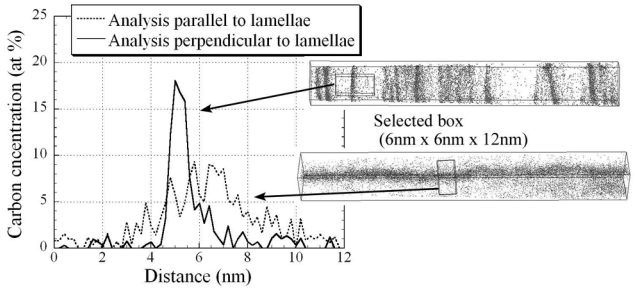

Fig. 8 Comparison of carbon concentration profiles obtained by probing directions parallel and perpendicular to the lamellae[19)]

with the aim of obtaining data about a specific region of steel wire with higher spatial resolution in a direction perpendicular to the pearlite lamellae, we prepared a needle specimen of the surface region of a steel wire in a direction perpendicular to the lamellae by using the lift-out method and analyzed the surface region using the needle specimen.[14, 19)] The specimen used was a high-carbon steel wire prepared by the Iron and Steel Institute of Japan as a common specimen (diameter: 50 μm; true strain: 5; composition: Fe-0.8C-0.2Si-0.5Mn (mass %)). **Fig. 6** shows FIB-SIM images illustrating the process of preparing the needle specimen. We cut out a very small square columnar block of the steel wire from a position 5 μm from the surface toward the center, fixed the block onto the needle post, and prepared a needle specimen using a ring-shaped scanning beam.[14, 18, 19)]

Fig. 7 shows the 3DAP analysis results. Fig. 7 (a) shows an FIM image of the wire surface before analysis. A ferrite region in the form of concentric rings is observed, indicating that the needle specimen was prepared in the direction perpendicular to the lamellae. Fig. 7 (b) shows 3D elemental maps. From the carbon distribution, the direction of the cementite lamellae and the spacing between them can clearly be seen. Fig. 7 (c) shows the carbon concentration profile. Although the carbon concentration at each cementite lamella differs, a maximum concentration of about 25 at.% was observed. **Fig. 8** shows a comparison of the carbon concentration profile of a specimen measured in the direction parallel to the lamellae with the carbon concentration profile of the same specimen measured in the direction perpendicular to the lamellae. The carbon concentration profile measured in the direction perpendicular to the lamellae shows a higher peak and a narrower width, indicating that measurement in the direction perpendicular to the lamellae gives a more accurate carbon concentration profile than conventional measurement in the direction parallel to the lamellae.[14, 18, 19)] Thus, our newly developed technology has made it possible to obtain more accurate information about the carbon concentration in high-carbon steel wire.

4.3 Specific depth position observation of WEL on a rail surface[23, 24)]

The white etching layer (WEL) that occurs on the rolling contact surface of a rail is a thin, hard layer that is considered to damage the rail surface. Therefore, clarifying the structure and the mechanism of WEL formation has been called for. Concerning the structure, some researchers consider that WEL is martensite,[25, 27)] while others maintain that WEL is a complete or incomplete form of nano-ferrite.[25, 26)] With respect to the mechanism of formation, too, there are still differences of opinion. Some think that WEL is the product of a transformation of austenite, which is formed in the rail by the heat of friction between the wheel and the rail and is subsequently cooled, while others suggest that WEL is the result of a change in the rail's structure caused by repetitive application of a large strain to the rail. On the other hand, it has been reported that WEL consists of more than one structure.[27)] Accordingly, it is necessary to elucidate the formation behavior of the entire WEL structure from the surface down to the bottom. Therefore, with the aim of obtaining some clues in our study into the cause of WEL, we carried out an atomic-level examination of the change in distribution of alloying elements in the depth direction of WEL by means of a 3DAP.[23, 24)]

The sample used was a piece of rail with WEL obtained from a conventional railway (JIS 60k-class rail manufactured in 1984; cumulative passing tonnage: 150 million tons). The principal chemical composition was Fe-0.70C-0.23Si-0.93Mn (mass %). The WEL of the rail sample was a thin layer (maximum thickness: 30 μm) lying along the track. Therefore, we prepared needle specimens for several different depths, from the top down to the bottom, of the WEL by using the lift-out method and FIB operation shown in **Fig. 9**.[23, 24)] The needle direction shown in the figure corresponds to the depth-wise direction. We accurately determined the depth-wise position of each of the needle specimens by referring to FIM images of the blocks before the FIB operation.

Fig. 10 shows an etching microphotograph of a WEL cross section containing micro-Vickers marks (the numerals indicate hardness HV), together with 3D elemental maps of the top, middle, and bottom of the WEL (the bold arrow in the figure indicates the surface direction). The WEL discontinuously shows greater hardness than the original pearlite structure of the rail. Even within the WEL,

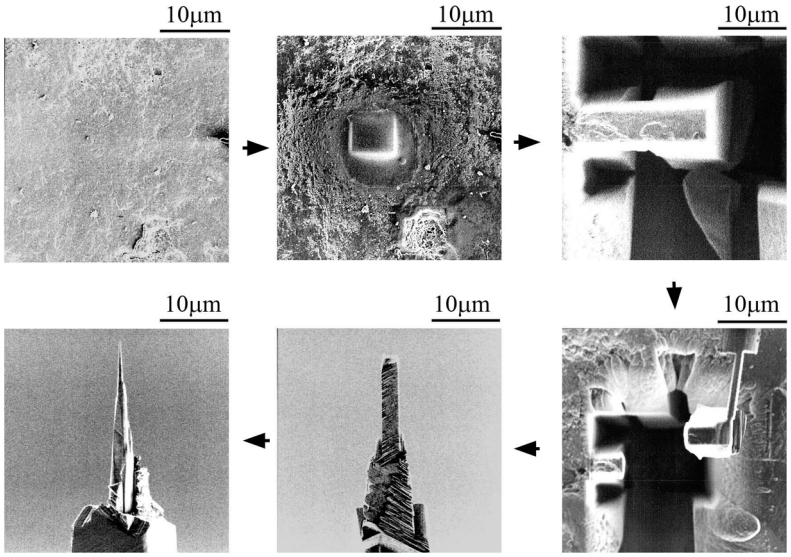

Fig. 9 Needle specimen fabrication process for atom probe analysis of the topmost surface of WEL[24)]

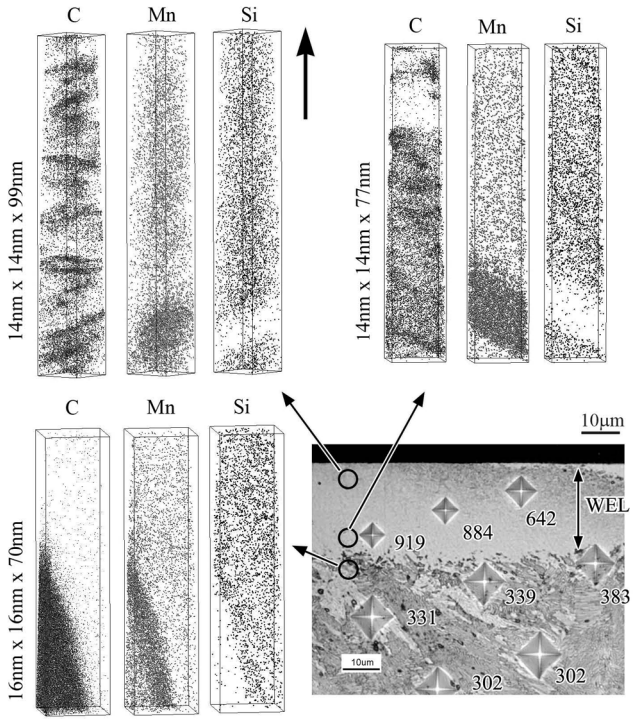

Fig. 10 Vickers hardness test results on the transverse section of WEL and 3D elemental maps of various depth positions[24)]

the hardness differs from one position to another, the lower part being harder than the upper part (topmost surface).[24, 27)] In the bottom of the WEL, the presence of lamellar cementite was clearly observed, which was found to be pearlite. The carbon distribution in the WEL was entirely different from that in the original pearlite. Namely, lamellar cementite was nonexistent, whereas solid solution, segregation, and precipitation of carbon were observed.[24)] Looking at the Mn and Si distributions, there were Mn-enriched and Si-depleted layers remaining in the positions corresponding to the lamellar cementite of the original pearlite. From the above distributions and lamella width, it was found that lamella refinement relative to the lamellar space of the original pearlite had not progressed much and that the amount of work near the WEL was smaller than expected.

Assuming that the rectangular concentration distribution of the Mn-enriched layer had changed because of diffusion, it was estimated that the temperature had reached at least 1200℃ in the upper part of the WEL and at least 1000℃ even in the lower part of the WEL. These estimates coincided with the result of calculating the heat of friction.[24)] It is considered that owing to the heat of friction between the wheels and the rail that is generated upon application of the brakes, etc., the rail reached the austenitizing temperature in a very short time, causing a martensitic transformation to take place in the process of cooling. Since the maximum rail temperature reached declines markedly as the distance from the surface of contact with the wheel increases, it can be seen that the WEL is a thin layer on the rail surface and that it has a clear boundary with the other part of the rail. It was considered that a WEL will occur under certain conditions that are met relatively infrequently. It was understood that the decline in hardness of the upper part of any WEL was due to the tempering of the formed WEL by passing trains.[24)]

As has been described above, by using technology to conduct depth-based observation of the surface of steel, we examined atomic-level change in local concentrations of the alloying elements within the prior cementite lamellae. On the basis of the examination results, we formed a hypothesis concerning the mechanism of formation of a WEL and performed model calculations to determine how the WEL is formed.

5. Conclusion

With the aim of expanding the scope of application of the 3DAP to steel materials, we developed a new technology for preparing needle specimens by pinpoint sampling of specific regions of steel. This new technology has made it possible to perform atomic-level observation of site-specific regions of steel that were extremely difficult to observe in the past. In addition, it should help solve a number of unresolved issues in steel metallurgy. Although steel materials have long been used, much has still to be learnt about them. In order to develop new steel materials with superior properties, we consider

it indispensable to utilize nanostructure analysis techniques, including 3DAP technology. It may be said that nano-analysis technology serves to link steel materials more closely to materials sciences. In this context, we firmly believe that it will become increasingly important in the future.

References

1) Miller, M. K., Cerezo, A., Hetherington, M. G., Smith, G. D. W.: Atom Probe Field Ion Microscopy. Oxford University Press, New York, 1996
2) Cerezo, A., Godfrey, T. J., Sijbrandij, S. J., Smith, G. D. W., Warren, P. J.: Rev. Sci. Instrum. 69, 49 (1998)
3) Miller, M. K.: Atom Probe Tomography: Analysis at the Atomic level, Kluwer Academic. Plenum Publishers, New York, 2000
4) Kelly, T. F., Miller, M. K.: Rev. Sci. Instrum. 78, 031101 (2007)
5) Gault, B., Vurpillot, F., Vella, A., Gilbert, M., Menand, A., Blavette, D., Deconihout, B.: Rev. Sci. Instrum. 77, 043705 (2006)
6) Larson, D. J., Foord, D. T., Petford-Long, A. K., Anthony, T. C., Rozdilsky, I. M., Cerezo, A., Smith, G. D. W.: Ultramicroscopy. 75, 145 (1998)
7) Larson, D. J., Foord, D. T., Petford-Long, A. K., Liew, H., Blamire, M. G., Cerezo, A., Smith, G. D. W.: Ultramicroscopy. 79, 287 (1999)
8) Seto, K., Larson, D. J., Warren, P. J., Smith, G. D. W.: Scripta Mater. 40, 1029 (1999)
9) Maruyama, N.: Ph.D Thesis. Oxford University, 2001
10) Takahashi, J., Sugiyama, M., Maruyama, N.: Shinnittetsu Giho. (381), 26 (2004)
11) Takahashi, J., Kawakami, K., Yamaguchi, Y., Sugiyama, M,: Ultramicroscopy. 107, 744 (2007)
12) Giannuzzi, L. A., Drown, J. L., Brown, S. R., Irwin, R. B., Stevie, F. A.: MRS Symp. Proc. 480, 10 (1997)
13) Kamino, T., Yaguchi, T., Ohnishi, T., Umemura, K., Tomimatsu, S.: Micro. Microanal. 6 (S2), 510 (2000)
14) Takahashi, J., Kawakami, K., Sugiyama, M., Tarui, T., Tashiro, H., Yamada, J.: CAMP-ISIJ. 18, 572 (2005)
15) Miller, M. K., Russell, K. F., Thompson, G. B.: Ultramicroscopy. 102, 287 (2005)
16) Gomer, R.: Field Emission and Field Ionization. Harvard University Press, Cambridge, MA, 1961
17) Sakurai, T., Müller, E. W.: J. Appl. Phys. 48, 2618 (1977)
18) Takahashi, J., Tarui, T.: Materia. 46, 813 (2007)
19) Takahashi, J., Kawakami, K., Tarui, T.: Ultramicroscopy. 109, 193 (2009)
20) Tarui, T., Maruyama, N.: Tetsu-to-Hagané. 90, 1031 (2004)
21) Danoix, F., Julien, D., Sauvage, X., Copreaux, J.: Mater. Sci. Eng. A. 250, 8 (1998)
22) Hong, M. H., Reynolds, Jr., W. T., Tarui, T., Hono, K.: Metall. Mater. Trans. A. 30A, 717 (1999)
23) Takahashi, J., Kawakami, K., Ueda, M.: Ferum. 14, 29 (2009)
24) Takahashi, J., Kawakami, K., Ueda, M.: Acta Mater. 58, 3602 (2010)
25) Österle, W., Rooch, H., Pyzalla, A., Wang, L.: Mater. Sci. Eng. A. 303, 150 (2001)
26) Lojkowski, W., Djahanbakhsh, M., Bürkle, G., Gierlotka, S., Zielinski, W., Fecht, H.-J.: Mater. Sci. Eng. A. 303, 197 (2001)
27) Zhang, H. W., Ohsaki, S., Mitao, S., Ohnuma, M., Hono, K.: Mater. Sci. Eng. A. 421, 191 (2006)

Jun TAKAHASHI
Chief Researcher, D.Eng.,
Materials Characterization Research Lab.,
Advanced Technology Research Laboratories
20-1, Shintomi, Futtsu, Chiba

Kazuto KAWAKAMI
Senior Researcher, D.Sc.,
Mathematical Science & Technology Research Lab.,
Advanced Technology Research Laboratories

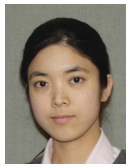

Yukiko KOBAYASHI
Researcher,
Materials Characterization Research Lab.,
Advanced Technology Research Laboratories

Junichi YAMADA
Group Leader,
Technical Service,
Nippon Steel Techno Research